Absence of microbiome in chronic infections impairs viral control without affecting CD8 T cell function

Miriam Kuhlmann[1], Daphne Del Carmen Kolland[2], Gustavo Pereira de Almeida[1], Christian Hoffmann[2,3], Madlaina von Hoesslin[1], Jacqueline Berner[1], Christine Wurmser[1], Caspar Ohnmacht[2*], and Dietmar Zehn[1*]

[1] Division of Animal Physiology and Immunology, School of Life Sciences Weihenstephan, Technical University of Munich, Freising, Germany.

[2] Center of Allergy and Environment (ZAUM) and Institute of Allergy Research, Technical University of Munich, School of Medicine, and Helmholtz Center Munich, Research Center for Environmental Health, Neuherberg, Germany.

[3] Food Research Center (ForC), Department of Food Science and Experimental Nutrition, School of Pharmaceutical Sciences, University of São Paulo, São Paulo, Brazil

* Corresponding authors:

Caspar Ohnmacht, Center of Allergy and Environment (ZAUM) and Institute of Allergy Research, Technical University of Munich, School of Medicine, and Helmholtz Center Munich, Research Center for Environmental Health; Neuherberg, Germany. Email: caspar.ohnmacht@helmholtz-muenchen.de

Dietmar Zehn, Division of Animal Physiology and Immunology, School of Life Sciences Weihenstephan, Technical University of Munich; Freising, Germany. Phone: +49 (8161) 71 3508, Email: dietmar.zehn@tum.de

ABSTRACT

Prolonged antigen exposure in chronic viral infections reduces the effector capacity of cytotoxic T cells - a phenomenon known as T cell exhaustion. High viral titer, strong TCR stimulation, and high antigen concentrations associated with strong inflammatory signals are known factors that promote the development of T cell exhaustion. A largely unexplored factor has been the influence of the microbiome on the development of T cell exhaustion. We report that T cell exhaustion progresses independently of the presence or absence of a bacterial microbiome in chronic lymphocytic choriomeningitis virus (LCMV) infections. Virus-specific CD8 T cells in germ-free mice showed high expression of the inhibitory receptor PD-1 and decreased cytokine production. Moreover, their global gene expression patterns, as determined by single-cell sequencing, were similar to those of cells in specific pathogen-free mice. In stark contrast to the phenotypic similarities, the absence of the microbiome delayed the partial viral control typically seen in chronic LCMV infections. Thus, our study demonstrates that the microbiome is dispensable for the induction of T cell exhaustion but critical for effector T cell function in chronic LCMV infections.

INTRODUCTION

Sustained antigen exposure, as occurs in chronic infections and tumors, triggers a differentiation program in T cells that is largely different from the program acquired by T cells during acute infection[1, 2]. Acute infection induce the proliferation and generation of large numbers of effector T cells that express high levels of effector molecules such as granzyme B, proinflammatory cytokines including tumor necrosis factor (TNF) and interferon gamma (IFNγ) while inhibitory receptors such as PD-1 and LAG-3 are only temporarily expressed. After infection has subsided, a population of memory cells can be detected in numbers largely exceeding the number of naïve T cells that were initially activated[3]. This memory population is maintained stably over long periods of time, and these cells mediate a strong recall response upon re-encounter with a similar or related pathogen. In contrast, although chronic infections also trigger strong activation and proliferation of pathogen-specific naïve T cells, the responding cells exhibit distinct phenotypic features including i) reduced expression of IFNγ and TNF, ii) stable expression of inhibitory receptors such as PD-1, and iii) characteristic global gene expression profiles and epigenetic marks[2, 4]. Cells with this phenotype are typically referred to as exhausted T cells. These exhausted T cell populations exhibit cellular dynamics that are largely different from T cells in acute infections and chronic infections are ultimately not associated with the formation of a typical memory compartment.

Exhausted T cell populations constitute the type of T cells that are available to be recruited for therapeutic purposes against malignant tumors or chronic infection. While their effector capacity is restricted compared to the cells found in acute infection, it is well

established that they still possess significant anti-tumor activity following their induced reactivation. Such reactivation is typically induced by blocking the inhibitory receptor-ligand systems that are expressed by exhausted T cells[5]. In fact, the demonstration that blocking PD-1 / PD-L1 with targeting antibodies was an important proof of principle demonstrating that anti-tumor potential is contained in exhausted T cells. Moreover, this finding paved the road for the line of therapy that is now known as checkpoint blockade[6].

Checkpoint blockade has proven to be extremely successful in many tumors compared to classical chemotherapy. Nevertheless, there are also a larger number of patients in whom checkpoint blockade has limited or no effect. These failures suggest that improving activation of the immune system and overcoming the phenomenon of T cell exhaustion by other means than with currently available reagents hold substantial promise for more efficient therapies. A prerequisite for such developments is a deeper understanding of the molecular mechanisms and host factors that determine T cell exhaustion. A largely unexplored question has been how the bacterial microbiome affects the development and the degree of T cell exhaustion that occurs in chronic infections and our ability to overcome this phenotype. Indeed, numerous reports indicate that the microbiome is a major factor influencing adaptive immunity but its impact on the prototypic model system of T cell exhaustion - lymphocytic choriomeningitis virus (LCMV) infections - remained elusive[7]. We therefore saw a need to systematically investigate, in well-controlled experimental systems, how the presence, or absence, or specific alterations of the bacterial microbiome affect the T cell response in chronic infections. We found that chronic LCMV infection leads to massive yet transient changes in the bacterial microbiome during the course of infection. Surprisingly, however, we found that CD8 T cell exhaustion was similar both with and

without a microbiome. Nevertheless, we detected massive changes in viral titers in immunopathology development in mice in the absence of a bacterial microbiome and in mice with a limited microbial consortium (oligoMM-12)[8]. These findings underscore that the microbiome has a critical impact on pathogen control and potential effector T cell function, whereas it does not affect phenotypic differentiation of virus-specific CD8 T cells in chronic infection.

RESULTS

Chronic infections induce massive but reversible changes in the bacterial microbiome

The intestinal microbiome shows a highly dynamic composition and is to a significant level constantly shaped and reshaped following bacterial exposure, alimentary alterations, antibiosis, or infections. We began our studies by looking at how the microbiome changes following exposure to acute and chronic LCMV infection - a prototypic model for studying T cell mediated immune responses in mice. The LCMV model has the advantage that several closely related strains exist that cause either acutely resolved infection or persisting chronic infection[7]. We used the LCMV armstrong strain, which causes an acute infection that is usually resolved within 5-10 days, and LCMV clone-13 or LCMV docile infections that persist for the life of the mice when applied at higher doses[9, 10].

To determine how the microbiome is affected during these infections, we horizontally collected fecal samples from mice before and at different time-points after the infection with acute LCMV armstrong or chronic LCMV clone-13 (**Fig. 1A**). We noted only minor changes in the alpha-diversity shown by both the Richness and the Shannon effective following acute infection (**Fig. 1B**). In contrast, there were massive changes in chronic infection (**Fig. 1B**). In fact, the microbiome of mice chronically infected with LCMV displayed a reduction in alpha-diversity and a shift in beta-diversity 8 days post infection which was not observed in acute infection (**Fig. 1C**). Importantly, this shift was only temporary and the microbiome shifted back to the original stage over time in chronic infection (**Fig. 1C, D**).

Similar expansion of virus-specific CD8 T cells in the spleen and small intestine in the absence of the microbiome

The strong changes in the microbiome over the course of the LCMV clone-13 infection raised our interest in determining if these changes impact the T cell response and in particular the T cell phenotype that arises in chronic infection. To assess the principle impact of the microbiome, we compared the response of T cells in specific pathogen-free (SPF) mice with mice that do not contain a bacterial microbiome (germ-free). We infected germ-free and SPF mice with LCMV clone-13 and used peptide-MHC tetramers presenting the LCMV derived gp33 peptide to assess the response of virus-specific CD8 T cells in chronic LCMV clone-13 infections. We found that SPF and germ-free mice contained similar frequencies (**Fig. 2A**) but slightly reduced total numbers of gp33 tetramer-positive T cells in both the spleen and in the lamina propria of the small intestine (SI-LP) in germ-free mice at 8 and 28 days post infection (**Fig. 2B**). We concluded that the presence of the microbiome enhances the total numbers of T cells in the mice and that as a consequence the number of gp33-specific T cells was increased but given the similar frequency of gp33-specific cells, we did not find evidence for altered expansion with and without a bacterial microbiome.

In contrast to our expectations, we did not detect major changes in the phenotype of gp33-specific T cells. Co-staining of gp33 tetramer-positive T cells obtained from the spleen and the small intestine on day 8 and 28 post LCMV clone-13 infection revealed similar mean fluorescence intensities of PD-1 expression under all conditions (**Fig. 3A, B**). Similarly, cells from both conditions showed a comparable effector phenotype, as they lacked CD127 expression (**Fig. 3C**) and remained negative for KLRG1 (**Fig. 3D**). Absence of KLRG1 is a typical

sign for exhausted effector T cells in chronic LCMV infection compared to cells found in acute and resolved LCMV infections, where a prominent KLRG1 expressing population can be detected[11]. Likewise, we also determined the cytokine secretion profile of gp33-specific T cells. Following brief ex-vivo restimulation with gp33 peptide plus subsequently performed intracellular staining, we detected similar IFNγ and TNF profiles in all conditions (**Fig. 4 and Supp. Fig. 1**). We noted that of the cytokine secreting cells, only a small fraction co-produced IFNγ and TNF while the majority of cytokine-positive cells produced only IFNγ and not TNF. Moreover, the IFNγ production of these cells was lower than of the IFNγ and TNF double producing cells (**Fig. 4**). These cytokine patterns are hallmark features of exhausted T cells in chronic LCMV infections[11]. Both strains, LCMV clone-13 and LCMV docile, induce chronic infections but the level of virus persistence and the level of T cell exhaustion is higher in LCMV docile compared to clone-13 infections. We therefore repeated our experiments using chronic LCMV docile infections. We noted a small tendency towards a slightly higher frequency of IFNγ producing cells but, overall, the phenotype of the T cells was again very similar in SPF and germ-free mice (**Fig. 5**). **We therefore conclude that LCMV-specific T cells acquire similar phenotypic signs of T cell exhaustion with and without a bacterial microbiome.**

LCMV-specific CD8 T cells show similar global gene expression profiles in germ-free and SPF mice

To explore more broadly the impact of the microbiome on LCMV specific CD8 T cells, we then decided to characterize these cells more thoroughly using an unbiased approach. We therefore collected ~1000-5000 gp33 tetramer-positive cells sorted from the lamina

propria of the small intestine and from the spleen of three germ-free and SPF mice and performed single cell-resolved RNA sequencing (**Fig. 6A**). A merged 2-dimensional UMAP representation of all samples is shown in **Figure 6B**. By unsupervised KNN clustering, we found two clusters specific for the spleen, three for the small intestine, while three clusters contained cells from both organs (**Fig. 6C**). Based on the expression of marker genes which are uniquely up- or downregulated in a specific cluster, we made the following assignments: Cluster S1 = circulating effector T cell cluster (i.e., KLF2□, CXCR3□, S1PR1□), Cluster S2 = progenitor T cell cluster (i.e., Tcf7(Tcf1)□, Id3□, Sell□, Cxcr5□, Ccr7□, GzmB□ not shown, ns), Cluster I1 = intestinal effector T cell cluster with signs of T cell exhaustion (Itgae(CD103)□, Cxcr6□ns, Pdcd1□ns, Lag-3□ns), Cluster I2 = intestinal effector T cell cluster (ITGAE(CD103)□, CD69□ns, Xcl1□, Icos□ns, Batf□ns, Nr4a1□, Nr4a2□ns, Nr4a3□), Cluster I3 = tissue resident intestinal T cells (ITGAE□), Cluster C1 = possibly dying cells (rich in mitochondrial genes), Cluster C2 = proliferating cluster (i.e., MKI67□, cell cycle genes□), Cluster C3 = effector T cell cluster (multiple effector T cell genes□) (**Fig. 6D**). T cells from SPF and germ-free mice had a similar percentage distribution among these clusters (**Fig. 6E**). **We conclude therefore that T cells are able to acquire an exhausted phenotype even in germ-free mice. These observations sustain our conclusion that the microbiome has a limited impact on the phenotype of CD8 T cells in an infection that goes along with a very strong inflammatory response.**

Functional impact of the microbiome on immunopathology in chronic LCMV infections

As a next step, we tested the pathogen control and effector function of CD8 T cells in germ-free, SPF, and also in mice that contained only the minimum oligo-mouse-microbiota

(oligoMM-12). This consortium includes 12 strains representing members of the major bacterial phyla in the murine gut. These are *Acutalibacter muris* KB18, *Flavonifractor plautii* YL31, *Enterocloster clostridioforme* YL32, *Blautia coccoides* YL58, *Clostridium innocuum* I46, *Limosilactobacillus reuteri* I49, *Enterococcus faecalis* KB1, *Bacteroides caecimuris* I48, *Muribaculum intestinale* YL27, *Bifidobacterium longum subsp. animalis* YL2, *Turicimonas muris* YL45 and *Akkermansia muciniphila* YL44. The consortium was developed initially as a stable minimal consortium[8]. After infecting these groups with LCMV clone-13 we surprisingly noted a major impairment of virus control in germ-free and oligoMM-12 mice compared to SPF mice. This difference was detectable in the spleen, liver, kidney, and small intestine 16 days post infection but it declined to more similar pathogen levels in all mice by day 28 post infection (**Fig. 7**). Of note, the 10-fold difference detected on day 16 constitutes a major difference in pathogen control in LCMV infections. We also noted a stronger difference in virus titers in systemic lymphoid organs such as the spleen. The kidneys are known to be an organ with very high LCMV titers and the organ with the highest level of virus persistence in chronic infections. Here, we noted a lower level of difference between the three groups, which might be linked to the fact that the kidney is less exposed to gut derived microbial stimuli than the liver but it could also result from the fact that virus titers are much higher in the kidneys and that differences in pathogen control potential have a lower impact in organs with very high LCMV titers. Moreover, we also confirmed that CD8 T cells have a similar phenotype in the different types of hosts including the oligoMM-12 mice (**Supp. Fig. 2**). **Overall, we conclude that while the bacterial microbiome is dispensable for the generation and modulation of an exhausted phenotype it critically impacts the level of pathogen control in chronic infections and likely the execution of effector function.**

DISCUSSION

We have addressed how the absence of a bacterial microbiome impacts the formation and the phenotype of exhausted T cells. Unexpectedly, we observed that T cells primed by chronic LCMV docile or LCMV clone-13 infections presented themselves with an identical phenotype and similar relative subset distribution with and without a bacterial microbiome. Even very deep expression profiling performed with the help of scRNA sequencing confirmed this picture. This outcome contrasts with other observations in which alterations in the composition of the microbiome went along with a strong impact on T cell phenotypes. For instance, Honda and colleagues identified a consortium of bacteria that is able to elicit stronger IFNγ induction in the CD8 T cell compartment that enhanced host resistance against *Listeria monocytogenes* infection and improved checkpoint inhibition efficacy in a tumor model[12]. The absence of microbial or dietary antigens was also shown to impact the composition of the T helper cell compartment as it prevented differentiation of regulatory T cells and caused a major bias towards Th2 differentiation[13]. Microbiota-dependent regulatory T cells constitute a cellular subset that links the microbiome to the regulation of immune responses during infections[14]. Such peripherally induced Treg cells, generated during a critical time window around weaning along with other microbiome-responding cell types, have also been proposed to counteract the general immune tone in germ-free mice from a type 2 bias and associated risk of atopic disorders to a more equilibrated immune system[15, 16, 17]. Moreover, certain bacterial species eventually colonizing the intestinal tract have been shown to mount robust Th1 cell responses[18, 19]. During chronic LCMV infection, however, absence of microbiome-induced Treg cells does not

seem to affect the virus-specific CD8 T cell response. We were also surprised about the similar outcome if one considers prior reports that structure of secondary lymphoid organs are underdeveloped or differentially organized in the absence of a microbiome[20, 21, 22]. For unclear reasons these deficits did not impair the ability to prime a profound CD8 T cell response to LCMV and for inducing T cell exhaustion. Whether virus-specific T helper cell responses are affected by microbial colonization is part of ongoing investigations but preliminary results suggest a more profound effect of the microbiome on this compartment.

We have started this project by looking at how the microbiome impacts the T cell phenotype in chronic infections after our laboratory has moved to a new animal facility. We noted changes in T cell phenotypes and therefore needed to adjust virus inoculation titers to obtain chronic LCMV infections in the new facility. In particular, findings that differences in animal husbandry lead to significant changes raised our interest in this topic[23]. Similarly, antibiotic treatments were also shown to massively alter the outcome of CD8 T cells during viral infection[24]. We thus suspected that a distinct microbial composition in the different animal facilities might have led to the phenotypic differences we have observed. However, our data argue against a microbial cause. Instead, we conclude that infections which go along with strong levels of an inflammatory response may create their own environment and that T cells can precede in this situation independently from the microbiome environment prior to the infection.

Despite these similarities in T cell phenotypes, we noted a massively altered level of anti-viral immunity, such that germ-free mice contained temporarily 10-fold higher virus titers than SPF mice. Particularly interesting was the fact that the impaired protection was

also obvious in mice colonized with the minimum oligoMM-12. Of note, it remains unresolved how and through which mechanism this lack of pathogen control occurs and it remains even unclear if the effect is mediated by CD8 T cells or unrelated mechanisms. So far, LCMV infections in germ-free mice were only performed acutely[25, 26]. Here, it was for instance observed that intracerebral infection resulted in better survival of germ-free mice compared to conventional mice[27]. These data are not easy to interpret as the intracerebral infection is different from the routes that are typically used for studying acute and chronic LCMV infection but also because of the lack of any insights into the T cell biology in this historic publication. However, it needs to be considered that LCMV is not a cytopathic virus such that high titers are tolerated by mice in the absence of T cells. In fact, immunopathology and lethal outcomes of LCMV infection are typically associated with too strong T cell responses[28]. It is therefore conceivable that SPF mice might contain slightly more total LCMV-specific T cells (as we have seen it, **Fig. 2**) and that these additional T cells might be sufficient to drive pathology while more effectively eliminating the virus. Matching our observation of impaired virus control in chronic infection in germ-free mice, similar outcomes were reported for acute infection in germ-free mice[25]. In contrast to the impaired virus clearance we have observed, it was also reported that specific alterations in the microbiome are also able to augment pathogen clearance[12].

It is well known that antibody responses develop slowly in chronic LCMV infections[29]. We therefore do not believe that different virus titers are caused by divergent B cell responses and differences in the level of neutralizing antibodies. In contrast, elevated virus titers might be linked to an impaired early containment of the infection such that the innate arm of the immune system might be less active without a microbiome and might thereby

impair early reduction of virus titers as it was reported for influenza and acute LCMV infections[30]. One possibility may be the microbiome-dependent effects on local microenvironments early after infection. For instance, LCMV infections are known for inducing high levels of type 1 interferons. Indeed, the microbiome has been shown to modulate tonic type 1 interferon levels which may be directly or indirectly critical for eliciting intact CD8 T cell responses and anti-viral immunity towards chikungunya virus infection[31]. In the chronic setting, we consider that strong type 1 interferon responses elicited by the LCMV infection dominate over any pre-existing condition but early after infection, microbiome-dependent pre-existing type-1 interferon levels may be important for the early containment of LCMV titers with consequences for chronic infection states. Interestingly, enteric virus infections with norovirus have been shown to sometimes overtake the beneficial effects of the microbiome with regards to protection from excessive intestinal injury and infection-induced pathology and this effect was dependent on type 1 interferon signaling[32]. Altogether, our results suggest that the phenomenon of CD8 T cell exhaustion can be readily induced in germ-free animals after chronic viral infection. Noteworthy, effector function and pathogen control may critically depend on the presence of a diverse microbiome. These results therefore underscore the need for future studies investigating additional links between the intestinal microbiome and regulation of anti-viral immunity to improve design of vaccination strategies and immune checkpoint therapies for boosting anti-tumor immunity.

MATERIAL AND METHODS

Mice: Specific pathogen-free (SPF) C57BL/6 mice were purchased from Charles River, germ-free (GF) C57BL/6 mice were provided by the Central Animal Facility (Hannover Medical School, Germany) and the Core Facility Gnotobiology (ZIEL - Institute for Food & Health, Technical University of Munich, Germany), and oligoMM-12 C57BL/6 mice were obtained from the Central Animal Facility (Hannover Medical School, Germany). P14[33] mice were provided by Annette Oxenius (ETH Zürich, Switzerland).

SPF mice were bred and maintained in specific pathogen-free facilities and infected in modified specific pathogen-free animal facilities at the Technical University of Munich (Germany). GF and oligoMM-12 mice were housed and infected in open cages within plastic film isolators and located in a room with a controlled environment at the Technical University of Munich (Germany).

Experiments were carried out in male or female mice that were at least six weeks old in strict accordance to the institutional and governmental regulations in Germany. All procedures were approved by the responsible veterinarian authorities of the Regierung von Oberbayern in Germany. Animals were randomly assigned to experimental groups which were non-blinded and no specific method was used to calculate sample sizes.

Infections and treatments: LCMV stocks were propagated in BHK-21 cells (provided by M. J. Bevan) cultured at 37 °C in Dulbecco's Modified Eagle Medium (DMEM) supplemented with 10% fetal calf serum (FCS). Frozen LCMV stocks were diluted in PBS (Gibco) and 2×10^5 pfu LCMV armstrong was injected intraperitoneally (i.p.), 5×10^6 pfu LCMV clone-13 or 2×10^4 pfu LCMV docile were injected intravenously (i.v.).

Measurement of viral burden: To determine virus load, tissues were harvested, weighted, and suspensions were shock-frozen and stored at -80 °C to release the virus. Levels of virus were determined by plaque forming assay[11]using Vero cells (provided by M. J. Bevan).

Isolation of lymphocytes from tissues: Spleens were dispersed into single-cell suspensions by mashing through a 100-µm nylon cell strainer (BD Falcon). Red blood cells were lysed with a hypotonic ammonium-chloride-potassium buffer.

To obtain SI-LP lymphocytes, residual adipose tissue and Peyer's patches were removed from the tissue. The SI was incubated in PBS containing 0.5 M EDTA for 30 min at 4 °C and afterwards washed in PBS and cut into small pieces. Digestion was performed by shaking in RPMI-medium (Gibco) with 240 mg/ml Liberase TL (Roche) and 150 µg/mL DNase I (Roche) at 37 °C for 60 min. Single-cell suspensions were obtained by filtering through a 100-µm nylon cell strainer. Cells were resuspended in 44% percoll (Cytiva) and underlaid with 67% percoll for density gradient centrifugation.

Purification of murine T cells for adoptive T cell transfers: Single-cell suspensions of splenocytes were obtained using a 100-µm nylon cell strainer (BD Falcon) and erythrocytes were lysed with a hypotonic ammonium-chloride-potassium buffer. $CD8^+$ T cells were purified by negative selection using the $CD8\alpha^+$ T cell isolation kit for mice (Miltenyi Biotech).

Surface and intracellular antibody staining and flow cytometry cell sorting of mouse cells: Blocking of unspecific antibody binding was achieved with 2.4G2 (BioXCell) and dead cells were stained using the Zombie NIR™ Fixable Viability Kit (Biolegend). Cells were stained with APC-conjugated MHC class I tetramers of $H\text{-}2D^b$ complexed with LCMV $gp_{33\text{-}41}$ (TCMetrix) for

1 h at 4 °C. Surface staining was performed for 30 min at 4 °C in PBS supplemented with 2% FCS (Sigma Aldrich) and 0.01% azide (Sigma-Aldrich) (FACS-buffer) using the following antibodies. Anti-CD45.1 (A20), anti-KLRG1 (2F1), anti-CD127 (A7R34), and anti-PD-1 (J43) were purchased from eBioscience, and anti-CD8a (53-6.7) and anti-CD103 (2EF) were obtained from Biolegend. Cells were fixed in PBS containing 2% formaldehyde for 15 min, then washed and resuspended in FACS-buffer. For intracellular cytokine staining, ~$3x10^6$ splenocytes were cultured in the absence or presence of gp_{33-41} for a total of 5 h at 37 °C. After 30 min, 7 µM brefeldin A was added. Following staining for surface antigens and fixation as described above, cells were permeabilized in PBS with 0.25% Saponin and 0.25% BSA (Perm-buffer). Staining with anti-IFNγ (XMG1.2) and anti-TNF (MP6-XT22) antibodies from eBioscience was performed for 40 min at 4 °C in Perm-buffer. For flow cytometry-based sorting, splenic and SI-LP cells were enriched for CD8 T cells using the mouse $CD8\alpha^+$ T cell isolation kit (Miltenyi Biotech). Virus-specific CD8 T cells were obtained by sorting of gp33-$Tetramer^+$ CD8 T cells using a FACSAria Fusion instrument (BD). Flow cytometry measurements were conducted on an LSR-Fortessa (BD). Data were analysed using FlowJo (TreeStar).

Single-cell RNA sequencing and analysis: Gene expression libraries for single cell sequencing were prepared by using the Chromium Next GEM Single Cell 3' Reagent Kit v3.1 and the 10x Chromium Controller (10x Genomics) following the manufacturer's protocol (CG000206 Rev D). Single Index Kit T Set A was used for multiplexing (i7 index read, 8bp). The samples were sequenced in a paired-end run (read 1: 28bp, read 2: 91bp) on a NovaSeq6000 platform

using S1 v1.5 (100 cycles) sequencing kits (Illumina). Bcl2fastq software (v2.20.0.422) was used for demultiplexing and generation of .fastq files allowing zero barcode-mismatches. Alignment of sequencing reads and gene counting with single-cell resolution were performed with 10x Genomics Cell Ranger v6.0.1 [34], using the default parameters and the pre-built mouse reference v2020-A (10x Genomics, Inc) based on mm10 - GENCODE vM23/Ensembl 98. Only cells with more than 1200 genes detected, less than 10% of mitochondrial genes and with UMI counts less than 3 standard deviations above the mean were kept for downstream analysis. Only data for genes detected in at least 3 cells in one of the samples were kept for further analysis. Contaminating cells were filtered out based on the average cluster expression of the marker genes Cd14, Lyz2, Fcgr3, Ms4a7, Fcer1g, Cst3, H2-Aa, Ly6d, Ms4a1, Ly6d, Cd19, Cd3e, Cd8a and mitochondrial genes. Raw read counts data from different tissues of the same donor were merged and normalized together using the R package sctransform v0.3.2 [35] (with glmGamPoi method). Downstream analysis was performed with the R package Seurat v4.0.1[36]. Anchors between replicates were identified on top 1000 highly variable genes and integration performed on first 20 dimensions. PCA was calculated on the top 1000 highly variable genes, KNN graph and UMAP were computed on the 30 nearest neighbors and first 20 PCA dimensions. Clusters were identified with the Louvain algorithm at resolution 0.36.

DNA extraction and 16S rRNA gene sequencing: Fecal samples were collected on dry ice immediately after sampling and stored at -80 °C. DNA was extracted with a modified protocol by Godon et al. [37] as previously described[38]. DNA was purified with the NucleoSpin gDNA Clean-up Kit (Machery-Nagel) following the manufacturer's protocol and DNA concentration determined by using a NanoDrop. The 16S rRNA gene was amplified by PCR using barcoded primers flanking the V3 and V4

hypervariable regions (341F, 785R)[39, 40]. Sequencing was performed on the Illumina MiSeq platform according to the manufacturer's instructions. Demultiplexed FASTQ files were transformed into Operational Taxonomic Unit (OTU) tables using the Integrated Microbial Next Generation Sequencing platform[41] (trimming of five nucleotides at the 5' and 3' end, minimum length: 300, maximum length: 600, filtering threshold of 0.25%). Downstream analysis was performed using the R pipeline Rhea[42]. Alpha-Diversity was calculated as species richness and Shannon effective number of species. Distance matrix for beta-diversity was calculated based on the generalized UniFrac approach[43]**.** Statistical analysis was performed by permutational multivariate analysis of variance (PERMANOVA).

General data analyses: Statistical analyses were performed with Prism 9.0 (Graphpad Software). Mann-Whitney test and unpaired t-test were used according to the type of experiment. P value < 0.05 was considered significant; p value > 0.05 was considered not significant.

REFERENCES

1. Blank, C.U. *et al.* Defining 'T cell exhaustion'. *Nat Rev Immunol* **19**, 665-674 (2019).

2. McLane, L.M., Abdel-Hakeem, M.S. & Wherry, E.J. CD8 T Cell Exhaustion During Chronic Viral Infection and Cancer. *Annu Rev Immunol* **37**, 457-495 (2019).

3. Zehn, D., Thimme, R., Lugli, E., de Almeida, G.P. & Oxenius, A. 'Stem-like' precursors are the fount to sustain persistent CD8(+) T cell responses. *Nat Immunol* **23**, 836-847 (2022).

4. Kallies, A., Zehn, D. & Utzschneider, D.T. Precursor exhausted T cells: key to successful immunotherapy? *Nat Rev Immunol* **20**, 128-136 (2020).

5. Barber, D.L. *et al.* Restoring function in exhausted CD8 T cells during chronic viral infection. *Nature* **439**, 682-687 (2006).

6. Wolchok, J.D. *et al.* Nivolumab plus ipilimumab in advanced melanoma. *N Engl J Med* **369**, 122-133 (2013).

7. Zehn, D. & Wherry, E.J. Immune Memory and Exhaustion: Clinically Relevant Lessons from the LCMV Model. *Adv Exp Med Biol* **850**, 137-152 (2015).

8. Brugiroux, S. *et al.* Genome-guided design of a defined mouse microbiota that confers colonization resistance against Salmonella enterica serovar Typhimurium. *Nat Microbiol* **2**, 16215 (2016).

9. Ahmed, R., Salmi, A., Butler, L.D., Chiller, J.M. & Oldstone, M.B. Selection of genetic variants of lymphocytic choriomeningitis virus in spleens of persistently infected mice. Role in suppression of cytotoxic T lymphocyte response and viral persistence. *J Exp Med* **160**, 521-540 (1984).

10. Moskophidis, D., Lechner, F., Pircher, H. & Zinkernagel, R.M. Virus persistence in acutely infected immunocompetent mice by exhaustion of antiviral cytotoxic effector T cells. *Nature* **362**, 758-761 (1993).

11. Utzschneider, D.T. *et al.* T cells maintain an exhausted phenotype after antigen withdrawal and population reexpansion. *Nat Immunol* **14**, 603-610 (2013).

12. Tanoue, T. *et al.* A defined commensal consortium elicits CD8 T cells and anti-cancer immunity. *Nature* **565**, 600-605 (2019).

13. Pircher, H., Rohrer, U.H., Moskophidis, D., Zinkernagel, R.M. & Hengartner, H. Lower receptor avidity required for thymic clonal deletion than for effector T-cell function. *Nature* **351**, 482-485 (1991).

14. Zheng, G.X. *et al.* Massively parallel digital transcriptional profiling of single cells. *Nat Commun* **8**, 14049 (2017).

15. Hafemeister, C. & Satija, R. Normalization and variance stabilization of single-cell RNA-seq data using regularized negative binomial regression. *Genome Biol* **20**, 296 (2019).

16. Hao, Y. *et al.* Integrated analysis of multimodal single-cell data. *Cell* **184**, 3573-3587 e3529 (2021).

ACKNOWLEDGMENTS

We thank C. Amette, B. Dötterböck, and W. Schmid for technical assistance; and C. Lechner for animal husbandry and the SFB1371 for providing the infrastructure to perform gnotobiotic experiments.

FUNDING

Work in the D.Z. laboratory was funded by the Deutsche Forschungsgemeinschaft (DFG, German Research Foundation) – Projektnummer 395357507 – SFB 1371 and supported by a "European Research Council consolidator grant" (ToCCaTa). The C.O. laboratory was supported by grants from the Deutsche Forschungsgemeinschaft (DFG) – Projektnummer 395357507 – SFB 1371 and grant number OH 282/1-2 within FOR2599 and further supported by a "European Research Council starting grant" (project number 716718).

AUTHOR CONTRIBUTION

Conceptualization: DZ, MK, CO; Formal analysis: MK, GPDA, MVH, DCK; Funding acquisition: DZ and CO; Investigation: MK, DCK, MVH, JB, CW; Methodology: MK; Visualization: MK, DZ; Writing: DZ, MK, CO

COMPETING INTERESTS

Authors declare that they have no competing interests.

DATA AND MATERIALS AVAILABILITY

All data will be made available upon publication. Next-generation sequencing data for this study have been deposited in the NCBI GEO repository with accession number XXXX.

FIGURE LEGENDS

Figure 1. Microbiome dynamics during acute (armstrong) and chronic LCMV (clone-13) infections. SPF C57BL/6 mice were infected with LCMV armstrong (blue) or LCMV clone-13 (green). Stool samples were collected one day before and 8, 17, and 24 days after infection (dpi) as illustrated in (**A**). **B**) Plots represent the alpha-diversity of the microbiome of the different time-points as the richness and the Shannon effective. **C**) The metaNMDS plot shows the beta-diversity of all microbiota in both infection models; dots represent individual mice. Samples are grouped according to the time-point at which they were taken.

Figure 2: Similar expansion and maintenance kinetic of virus-specific CD8 T cells in chronic infections with and without the microbiome. Experimental design: Germ-free (GF) and SPF C57BL/6 mice were infected with LCMV clone-13 and analyzed on day 8 or day 28 after infection. **A**) Representative, CD8 gated flow cytometry plots showing the frequency of tetramer$^+$ cells of germ-free and SPF mice on day 8 and d28 after infection in the spleen and the lamina propria of the small intestine (SI-LP). The dot plots on the right show the frequencies for all germ-free (red) and SPF (black) mice. **B**) Enumeration of total tetramer$^+$ cells of germ-free and SPF mice on day 8 and d28 after infection in the spleen and per centimeter of the SI-LP. Colors as indicated in (A). All data are representative for at least two independently performed experiments with at least $n \geq 5$, symbols indicate individual mice; horizontal lines show the mean. P values are from unpaired t-test.

Figure 3: Similar phenotype of virus-specific CD8 T cells in chronic infections with and without the microbiome. Experimental design: Germ-free (GF) and SPF C57BL/6 mice were

infected with LCMV clone-13 and analyzed on day 8 or day 28 after infection. **A** and **B**) Representative, tetramer$^+$ gated histograms showing the expression of PD-1 for germ-free and SPF mice on day 8 and d28 after infection in the spleen (A) and SI-LP (B). The dot plots at the bottom show the MFI of PD-1 on tetramer$^+$ cells for all germ-free and SPF mice. **C**) Representative, tetramer$^+$ gated histograms showing expression of CD127 for germ-free (red) and SPF (black) mice on day 8 and d28 after infection in the spleen. The dot plot at the bottom shows the frequencies of CD127$^+$ cells for all germ-free and SPF mice, Color coding as indicated in (A). **D**) Representative, tetramer$^+$ gated histograms showing the expression of KLRG1 for germ-free and SPF mice on day 8 and d28 after infection in the spleen. The dot plot at the bottom shows the frequencies of KLRG1$^+$ cells for all germ-free and SPF mice. Colors as indicated in (A). All data are representative for at least two independently performed experiments with at least n ≥ 5, symbols indicate individual mice; horizontal lines show the mean. P values are from unpaired t-test.

Figure 4: Absence of a microbiome reduces the cytokine secretion capacity of virus-specific CD8 T cells in the intestine. Experimental design: Germ-free (GF) and SPF C57BL/6 mice were infected with LCMV clone-13 and analyzed on day 8 or day 28 after infection. **A** and **B**) Representative, CD8 gated flow cytometry plots showing the frequency of IFNγ and TNF expressing cells of germ-free and SPF mice on day 8 and d28 after infection after restimulation with gp_{33-41} in the spleen (A) and the SI-LP (B). The dot plots at the bottom show the frequencies of IFNγ expressing (left) CD8 T cells and frequencies of TNF$^+$ of IFNγ expressing (right) CD8 T cells for all germ-free (red) and SPF (black) mice. All data are representative for at least two independently performed experiments with at least n ≥ 5,

symbols indicate individual mice; horizontal lines show the mean. P values are from unpaired t-test.

Figure 5: Kinetic and phenotype of virus-specific CD8 T cells is independent of the microbiome in LCMV docile infections. Experimental design: Germ-free (GF) and SPF C57BL/6 mice were infected with LCMV docile and analyzed on day 16 after infection. **A**) Frequencies of tetramer$^+$ cells of germ-free (red) and SPF mice (black) in the spleen and SI-LP. **B**) Numbers of tetramer$^+$ cells of germ-free and SPF mice in the spleen (left) and per centimeter of the SI-LP (right). Colors as indicated in (A). **C**) Frequencies of KLRG1$^+$ and CD127$^+$ and MFI of PD-1 of tetramer$^+$ cells for germ-free and SPF mice in the spleen (KLRG1, CD127 and PD-1) and the SI-LP (PD-1). Colors as indicated in (A). **D**) Frequencies of IFNγ expressing (left) CD8 T cells and frequencies of TNF$^+$ of IFNγ expressing (right) CD8 T cells for germ-free and SPF mice. Colors as indicated in (A). All data are representative for at least two independently performed experiments with at least n ≥ 5, symbols indicate individual mice; horizontal lines show the mean. P values are from unpaired t-test.

Figure 6: Single-cell RNA sequencing reveals a limited impact of the microbiome on the transcriptional profile of virus-specific CD8 T cells. A) Experimental design: Germ-free (GF) and SPF C57BL/6 mice were infected with LCMV docile and tetramer$^+$ CD8 T cells were sorted 16 days post infection from the spleen and SI-LP. **B**) Uniform Manifold Approximation and Projection (UMAP) showing the distribution of cells originating from the spleen (SP) and small intestine lamina propria (SI) in GF and SPF mice. **C**) UMAP showing the clusters identified by unsupervised KNN: 2 clusters specific for the spleen (S), 3 clusters specific for

the small intestine (I), and 3 common clusters (C). **D**) Heat map shows genes of interest selected from the top-20 marker genes of the individual clusters. **E**) Plots show the percentage wise distribution of cells of all analyzed samples into these clusters.

Figure 7: Absence of the microbiome significantly reduces virus control in chronic LCMV infections. Experimental design: Germ-free (GF, red), SPF (black) and oligoMM-12 reconstituted (OMM12, blue) C57BL/6 mice were infected with LCMV clone-13. Viral titers in the spleen, liver, kidney and SI-LP were assessed on day 16 or day 28 after infection. All data are representative for at least two independently performed experiments with at least n ≥ 4, symbols indicate individual mice; horizontal lines show the mean. P values are from unpaired t-test or Mann-Whitney test (*p value < 0.05, **p value < 0.01, ***p value < 0.001, ****p value < 0.0001).

1. Blank, C.U. *et al.* Defining 'T cell exhaustion'. *Nat Rev Immunol* **19**, 665-674 (2019).

2. McLane, L.M., Abdel-Hakeem, M.S. & Wherry, E.J. CD8 T Cell Exhaustion During Chronic Viral Infection and Cancer. *Annu Rev Immunol* **37**, 457-495 (2019).

3. Zehn, D., Thimme, R., Lugli, E., de Almeida, G.P. & Oxenius, A. 'Stem-like' precursors are the fount to sustain persistent CD8(+) T cell responses. *Nat Immunol* **23**, 836-847 (2022).

4. Kallies, A., Zehn, D. & Utzschneider, D.T. Precursor exhausted T cells: key to successful immunotherapy? *Nat Rev Immunol* **20**, 128-136 (2020).

5. Barber, D.L. *et al.* Restoring function in exhausted CD8 T cells during chronic viral infection. *Nature* **439**, 682-687 (2006).

6. Wolchok, J.D. *et al.* Nivolumab plus ipilimumab in advanced melanoma. *N Engl J Med* **369**, 122-133 (2013).

7. Zehn, D. & Wherry, E.J. Immune Memory and Exhaustion: Clinically Relevant Lessons from the LCMV Model. *Adv Exp Med Biol* **850**, 137-152 (2015).

8. Brugiroux, S. *et al.* Genome-guided design of a defined mouse microbiota that confers colonization resistance against Salmonella enterica serovar Typhimurium. *Nat Microbiol* **2**, 16215 (2016).

9. Ahmed, R., Salmi, A., Butler, L.D., Chiller, J.M. & Oldstone, M.B. Selection of genetic variants of lymphocytic choriomeningitis virus in spleens of persistently infected mice. Role in suppression of cytotoxic T lymphocyte response and viral persistence. *J Exp Med* **160**, 521-540 (1984).

10. Moskophidis, D., Lechner, F., Pircher, H. & Zinkernagel, R.M. Virus persistence in acutely infected immunocompetent mice by exhaustion of antiviral cytotoxic effector T cells. *Nature* **362**, 758-761 (1993).

11. Utzschneider, D.T. *et al.* T cells maintain an exhausted phenotype after antigen withdrawal and population reexpansion. *Nat Immunol* **14**, 603-610 (2013).

12. Tanoue, T. *et al.* A defined commensal consortium elicits CD8 T cells and anti-cancer immunity. *Nature* **565**, 600-605 (2019).

13. Kim, K.S. *et al.* Dietary antigens limit mucosal immunity by inducing regulatory T cells in the small intestine. *Science* **351**, 858-863 (2016).

14. Ohnmacht, C. *et al.* MUCOSAL IMMUNOLOGY. The microbiota regulates type 2 immunity through RORgammat(+) T cells. *Science* **349**, 989-993 (2015).

15. Cahenzli, J., Koller, Y., Wyss, M., Geuking, M.B. & McCoy, K.D. Intestinal microbial diversity during early-life colonization shapes long-term IgE levels. *Cell Host Microbe* **14**, 559-570 (2013).

16. Josefowicz, S.Z. *et al.* Extrathymically generated regulatory T cells control mucosal TH2 inflammation. *Nature* **482**, 395-399 (2012).

17. Al Nabhani, Z. *et al.* A Weaning Reaction to Microbiota Is Required for Resistance to Immunopathologies in the Adult. *Immunity* **50**, 1276-1288 e1275 (2019).

18. Atarashi, K. *et al.* Ectopic colonization of oral bacteria in the intestine drives TH1 cell induction and inflammation. *Science* **358**, 359-365 (2017).

19. Nagayama, M. *et al.* TH1 cell-inducing Escherichia coli strain identified from the small intestinal mucosa of patients with Crohn's disease. *Gut Microbes* **12**, 1788898 (2020).

20. Littman, D.R. & Pamer, E.G. Role of the commensal microbiota in normal and pathogenic host immune responses. *Cell Host Microbe* **10**, 311-323 (2011).

21. Smith, K., McCoy, K.D. & Macpherson, A.J. Use of axenic animals in studying the adaptation of mammals to their commensal intestinal microbiota. *Semin Immunol* **19**, 59-69 (2007).

22. Abolins, S. *et al.* The comparative immunology of wild and laboratory mice, Mus musculus domesticus. *Nat Commun* **8**, 14811 (2017).

23. Ericsson, A.C. *et al.* The influence of caging, bedding, and diet on the composition of the microbiota in different regions of the mouse gut. *Sci Rep* **8**, 4065 (2018).

24. Ichinohe, T. *et al.* Microbiota regulates immune defense against respiratory tract influenza A virus infection. *Proc Natl Acad Sci U S A* **108**, 5354-5359 (2011).

25. Ganal, S.C. *et al.* Priming of natural killer cells by nonmucosal mononuclear phagocytes requires instructive signals from commensal microbiota. *Immunity* **37**, 171-186 (2012).

26. Labarta-Bajo, L. *et al.* CD8 T cells drive anorexia, dysbiosis, and blooms of a commensal with immunosuppressive potential after viral infection. *Proc Natl Acad Sci U S A* **117**, 24998-25007 (2020).

27. Szeri, I., Anderlik, P., Banos, Z. & Radnai, B. Decreased cellular immune response of germ-free mice. *Acta Microbiol Acad Sci Hung* **23**, 231-234 (1976).

28. Blattman, J.N., Wherry, E.J., Ha, S.J., van der Most, R.G. & Ahmed, R. Impact of epitope escape on PD-1 expression and CD8 T-cell exhaustion during chronic infection. *J Virol* **83**, 4386-4394 (2009).

29. Bergthaler, A. *et al.* Impaired antibody response causes persistence of prototypic T cell-contained virus. *PLoS Biol* **7**, e1000080 (2009).

30. Abt, M.C. *et al.* Commensal bacteria calibrate the activation threshold of innate antiviral immunity. *Immunity* **37**, 158-170 (2012).

31. Winkler, E.S. *et al.* The Intestinal Microbiome Restricts Alphavirus Infection and Dissemination through a Bile Acid-Type I IFN Signaling Axis. *Cell* **182**, 901-918 e918 (2020).

32. Kernbauer, E., Ding, Y. & Cadwell, K. An enteric virus can replace the beneficial function of commensal bacteria. *Nature* **516**, 94-98 (2014).

33. Pircher, H., Rohrer, U.H., Moskophidis, D., Zinkernagel, R.M. & Hengartner, H. Lower receptor avidity required for thymic clonal deletion than for effector T-cell function. *Nature* **351**, 482-485 (1991).

34. Zheng, G.X. *et al.* Massively parallel digital transcriptional profiling of single cells. *Nat Commun* **8**, 14049 (2017).

35. Hafemeister, C. & Satija, R. Normalization and variance stabilization of single-cell RNA-seq data using regularized negative binomial regression. *Genome Biol* **20**, 296 (2019).

36. Hao, Y. *et al.* Integrated analysis of multimodal single-cell data. *Cell* **184**, 3573-3587 e3529 (2021).

37. Godon, J.J., Zumstein, E., Dabert, P., Habouzit, F. & Moletta, R. Molecular microbial diversity of an anaerobic digestor as determined by small-subunit rDNA sequence analysis. *Appl Environ Microbiol* **63**, 2802-2813 (1997).

38. Reitmeier, S., Kiessling, S., Neuhaus, K. & Haller, D. Comparing Circadian Rhythmicity in the Human Gut Microbiome. *STAR Protoc* **1**, 100148 (2020).

39. Kozich, J.J., Westcott, S.L., Baxter, N.T., Highlander, S.K. & Schloss, P.D. Development of a dual-index sequencing strategy and curation pipeline for analyzing amplicon sequence data on the MiSeq Illumina sequencing platform. *Appl Environ Microbiol* **79**, 5112-5120 (2013).

40. Berry, D., Ben Mahfoudh, K., Wagner, M. & Loy, A. Barcoded primers used in multiplex amplicon pyrosequencing bias amplification. *Appl Environ Microbiol* **77**, 7846-7849 (2011).

41. Lagkouvardos, I. *et al.* IMNGS: A comprehensive open resource of processed 16S rRNA microbial profiles for ecology and diversity studies. *Sci Rep* **6**, 33721 (2016).

42. Lagkouvardos, I., Fischer, S., Kumar, N. & Clavel, T. Rhea: a transparent and modular R pipeline for microbial profiling based on 16S rRNA gene amplicons. *PeerJ* **5**, e2836 (2017).

43. Chen, J. *et al.* Associating microbiome composition with environmental covariates using generalized UniFrac distances. *Bioinformatics* **28**, 2106-2113 (2012).

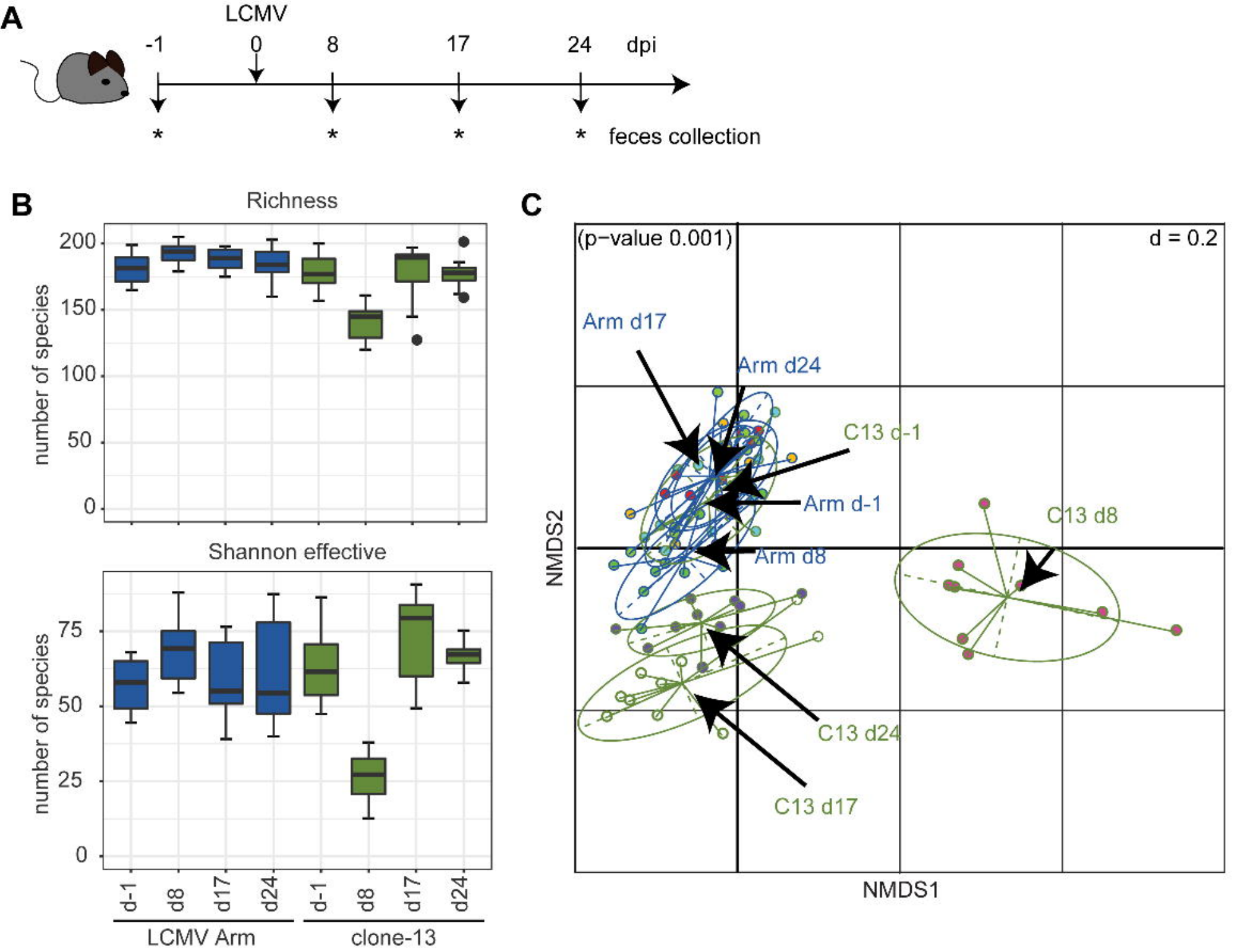
A
LCMV
-1
0
8
17
24
dpi
feces collection
B
Richness
number of species
200
150
100
50
0
Shannon effective
number of species
75
50
25
0
d-1
d8
d17
d24
d-1
d8
d17
d24
LCMV Arm
clone-13
C
(p−value 0.001)
d = 0.2
Arm d17
Arm d24
C13 d-1
Arm d-1
C13 d8
Arm d8
C13 d24
C13 d17
NMDS2
NMDS1

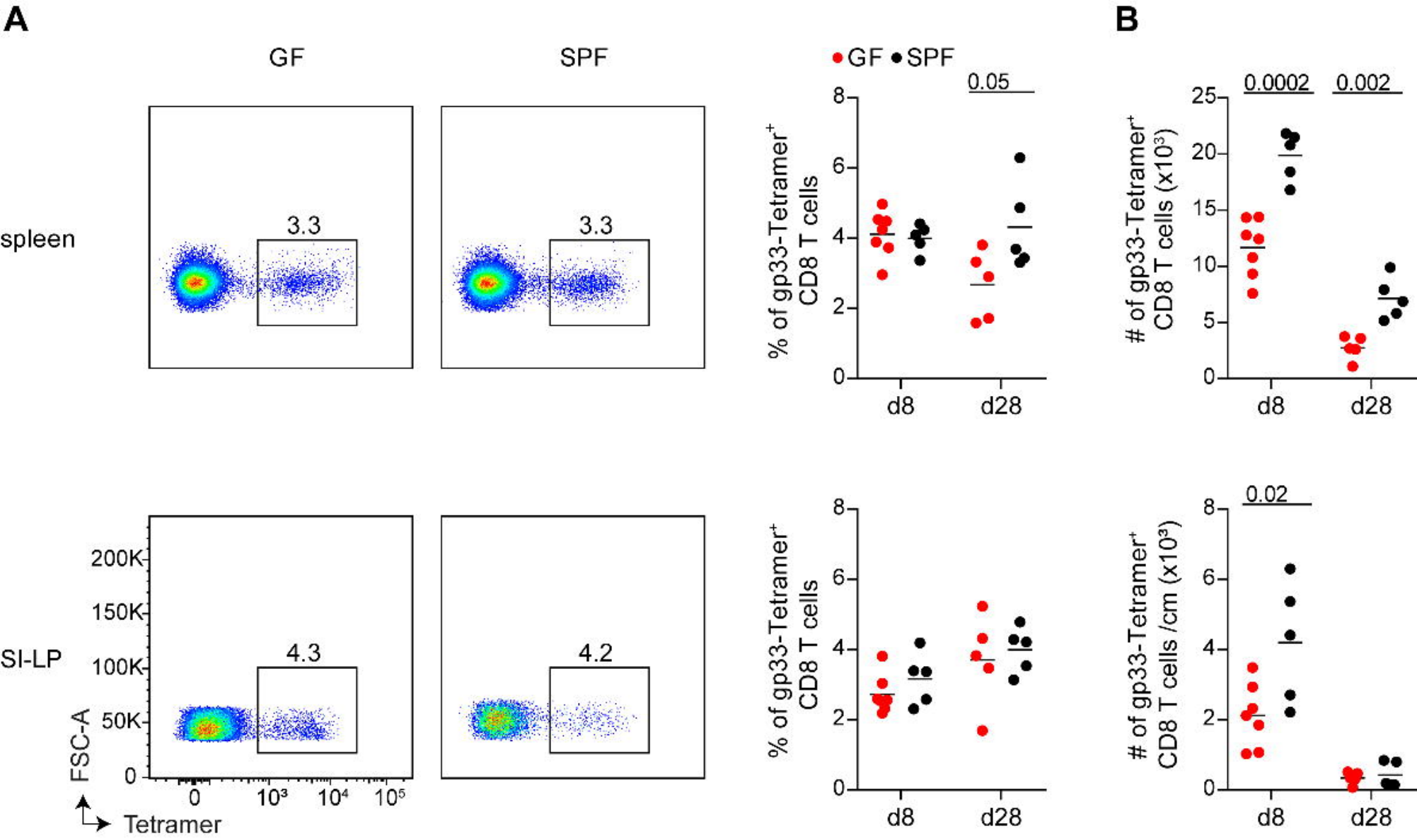
A
B
GF
SPF
GF SPF
spleen
SI-LP
3.3
3.3
4.3
4.2
200K
150K
100K
50K
0
FSC-A
0
10³
10⁴
10⁵
Tetramer
0.05
0.0002
0.002
0.02
% of gp33-Tetramer+ CD8 T cells
# of gp33-Tetramer+ CD8 T cells (x10³)
# of gp33-Tetramer+ CD8 T cells /cm (x10³)
d8
d28

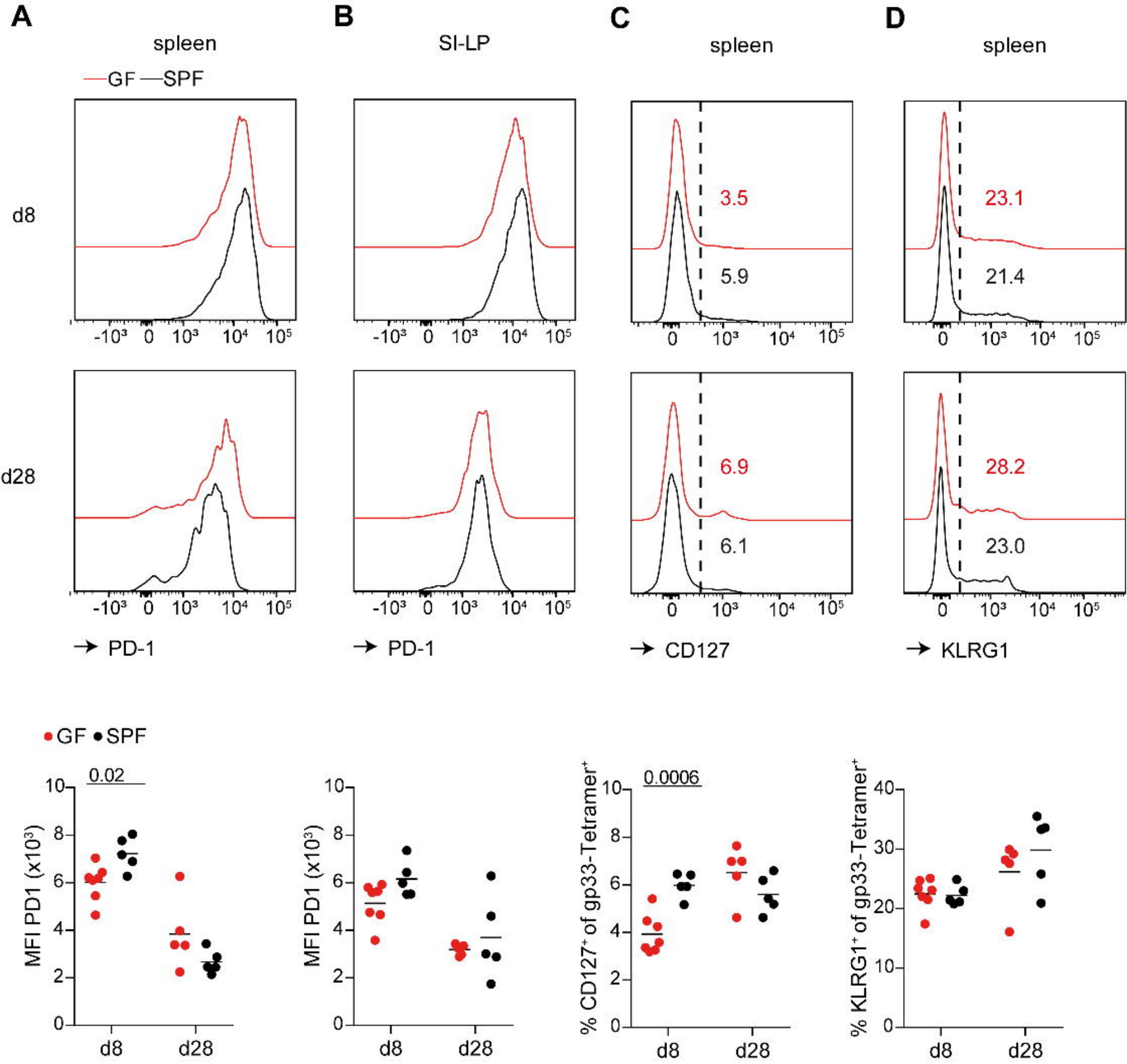
A
spleen
GF
SPF
d8
d28
-10³ 0 10³ 10⁴ 10⁵
→ PD-1
B
SI-LP
→ PD-1
C
spleen
3.5
5.9
6.9
6.1
0 10³ 10⁴ 10⁵
→ CD127
D
spleen
23.1
21.4
28.2
23.0
→ KLRG1
GF SPF
0.02
MFI PD1 (x10³)
0.0006
% CD127⁺ of gp33-Tetramer⁺
% KLRG1⁺ of gp33-Tetramer⁺
d8
d28

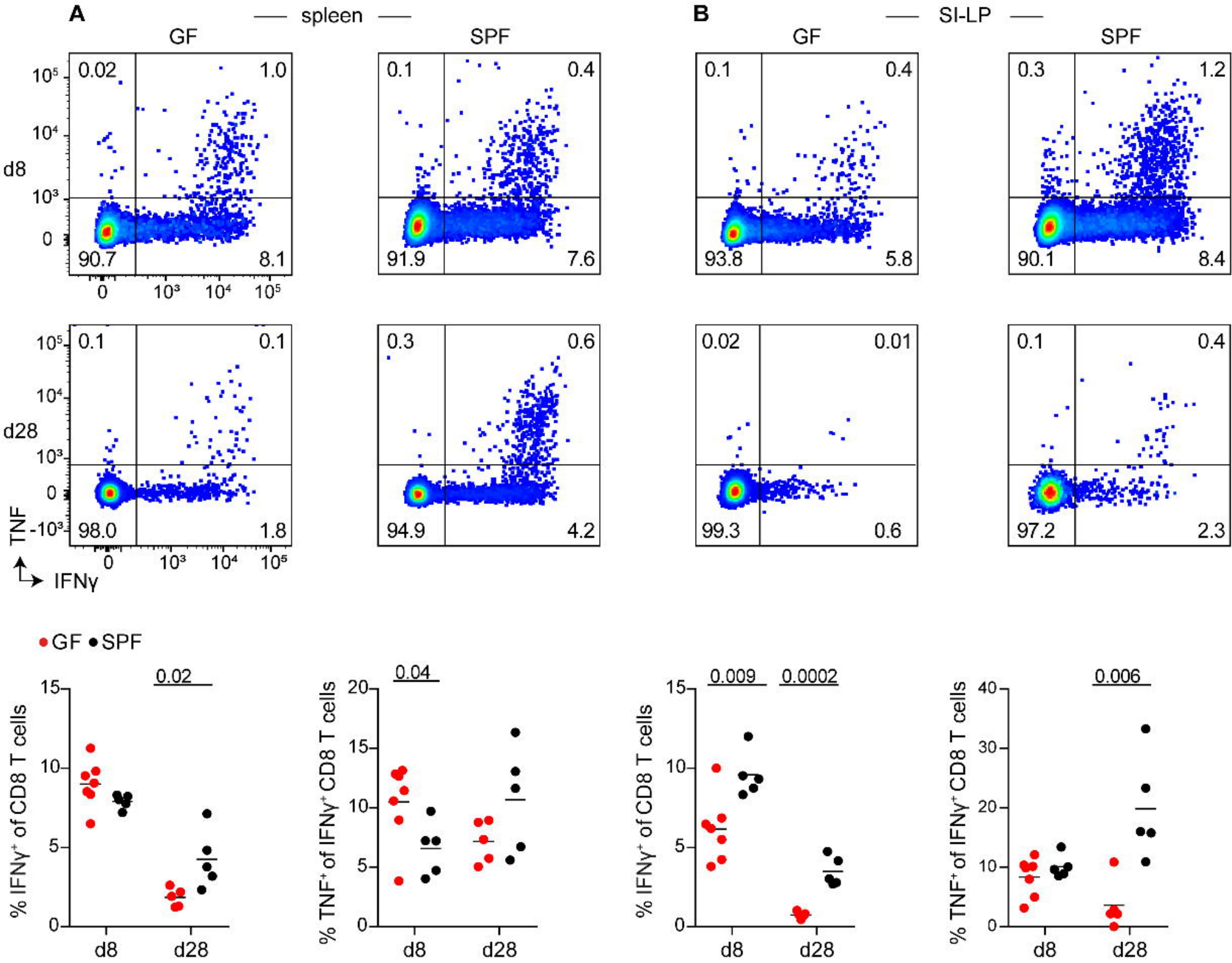
A
spleen
GF
SPF
B
SI-LP
GF
SPF
d8
d28
TNF
IFNγ
0.02
1.0
90.7
8.1
0.1
0.4
91.9
7.6
0.1
0.4
93.8
5.8
0.3
1.2
90.1
8.4
0.1
0.1
98.0
1.8
0.3
0.6
94.9
4.2
0.02
0.01
99.3
0.6
0.1
0.4
97.2
2.3
GF SPF
% IFNγ+ of CD8 T cells
% TNF+ of IFNγ+ CD8 T cells
% IFNγ+ of CD8 T cells
% TNF+ of IFNγ+ CD8 T cells
0.02
0.04
0.009
0.0002
0.006
d8
d28

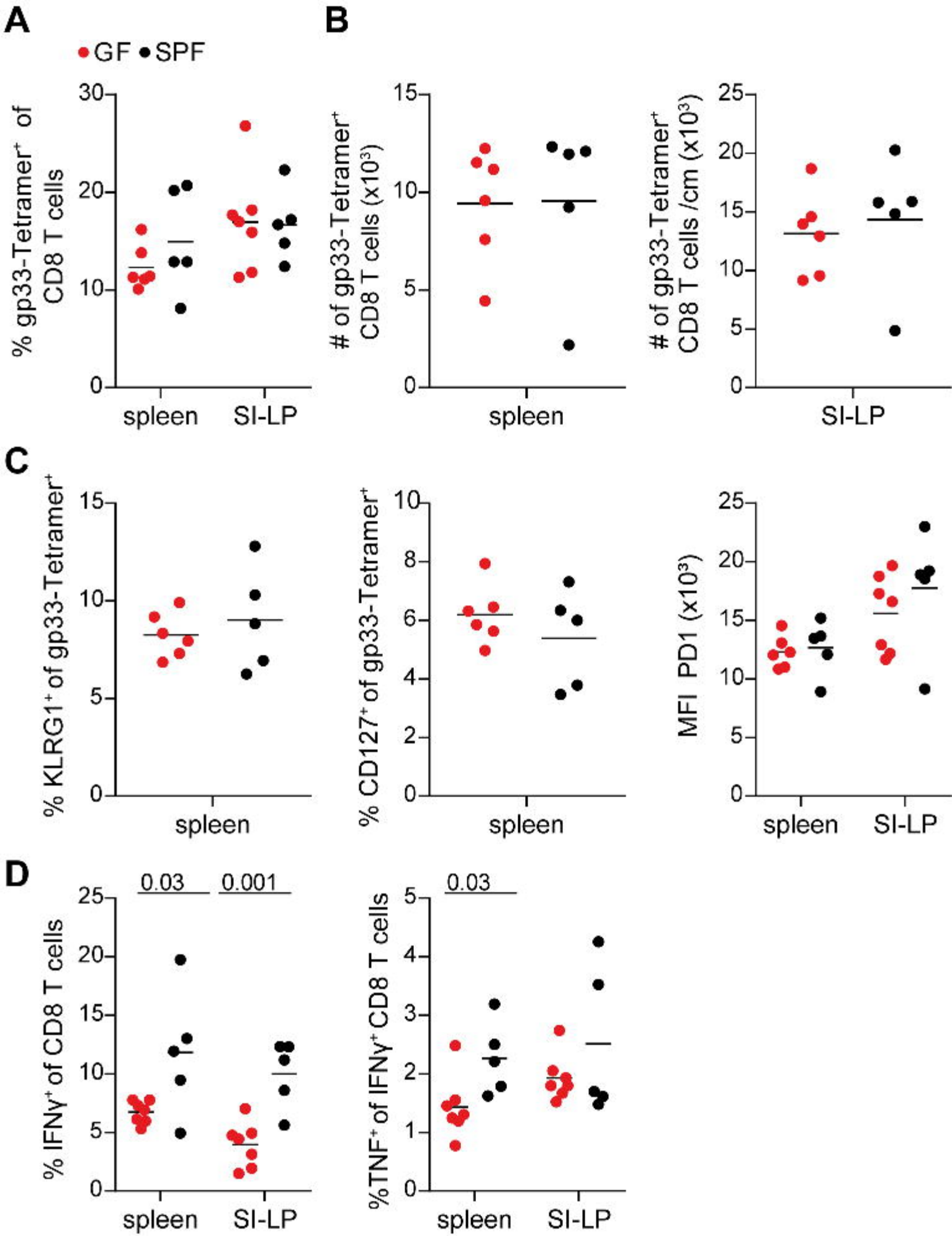
A
GF
SPF
% gp33-Tetramer+ of CD8 T cells
spleen
SI-LP
B
# of gp33-Tetramer+ CD8 T cells (x10³)
spleen
# of gp33-Tetramer+ CD8 T cells /cm (x10³)
SI-LP
C
% KLRG1+ of gp33-Tetramer+
spleen
% CD127+ of gp33-Tetramer+
spleen
MFI PD1 (x10³)
spleen
SI-LP
D
0.03
0.001
% IFNγ+ of CD8 T cells
spleen
SI-LP
0.03
%TNF+ of IFNγ+ CD8 T cells
spleen
SI-LP

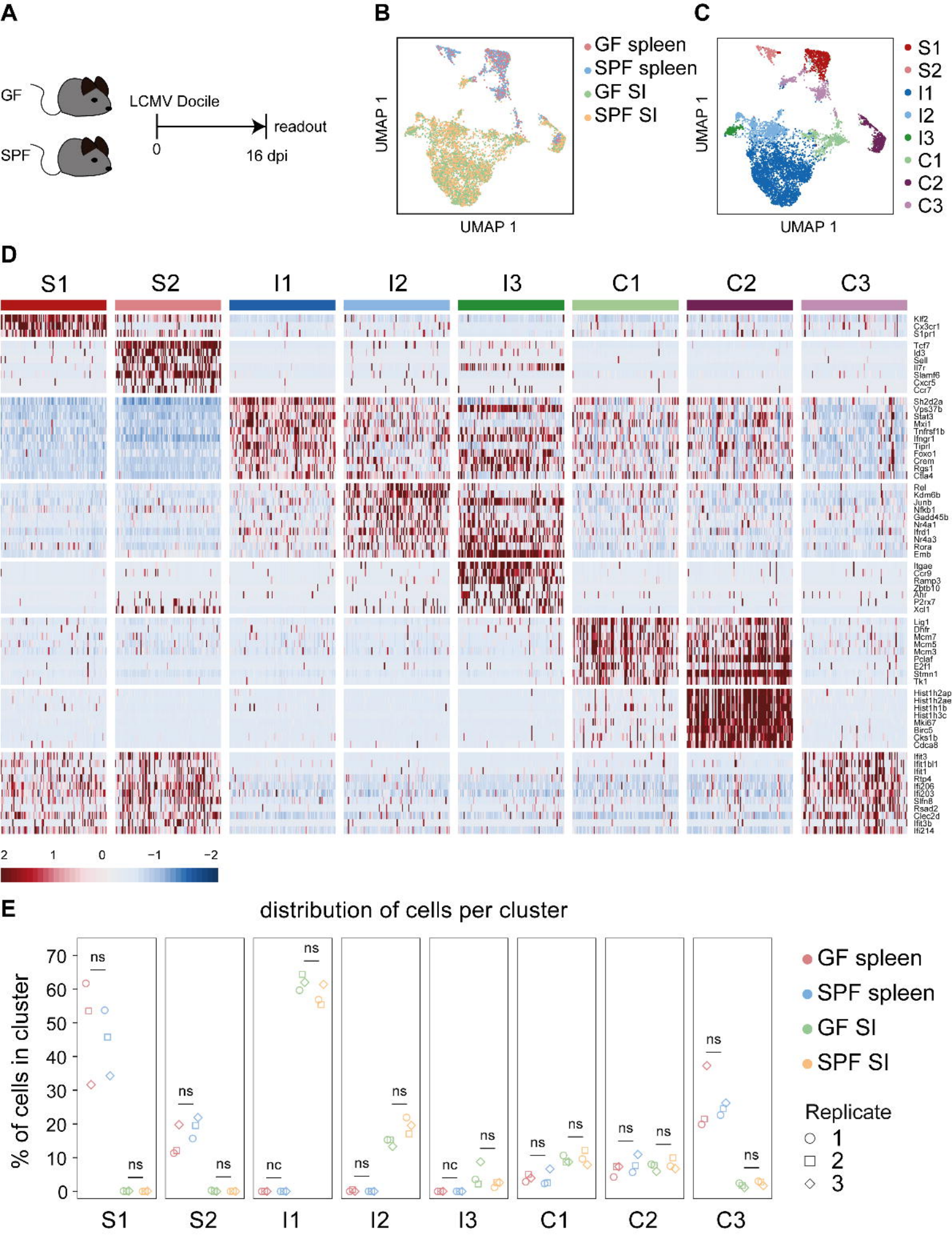
A
GF
SPF
LCMV Docile
0
16 dpi
readout
B
GF spleen
SPF spleen
GF SI
SPF SI
UMAP 1
UMAP 1
C
S1
S2
I1
I2
I3
C1
C2
C3
UMAP 1
UMAP 1
D
S1
S2
I1
I2
I3
C1
C2
C3
Klf2
Cx3cr1
S1pr1
Tcf7
Id3
Sell
Il7r
Slamf6
Cxcr5
Ccr7
Sh2d2a
Vps37b
Stat3
Mxi1
Tnfrsf1b
Ifngr1
Tiprl
Foxo1
Crem
Rgs1
Ctla4
Rel
Kdm6b
Junb
Nfkb1
Gadd45b
Nr4a1
Ifrd1
Nr4a3
Rora
Emb
Itgae
Ccr9
Ramp3
Zbtb10
Ahr
P2rx7
Xcl1
Lig1
Dhfr
Mcm7
Mcm5
Mcm3
Pclaf
E2f1
Stmn1
Tk1
Hist1h2ap
Hist1h2ae
Hist1h1b
Hist1h3c
Mki67
Birc5
Cks1b
Cdca8
Ifit3
Ifit1bl1
Ifit1
Rtp4
Ifi206
Ifi203
Slfn8
Rsad2
Clec2d
Ifit3b
Ifi214
2
1
0
−1
−2
E
distribution of cells per cluster
% of cells in cluster
70
60
50
40
30
20
10
0
ns
nc
S1
S2
I1
I2
I3
C1
C2
C3
GF spleen
SPF spleen
GF SI
SPF SI
Replicate
1
2
3

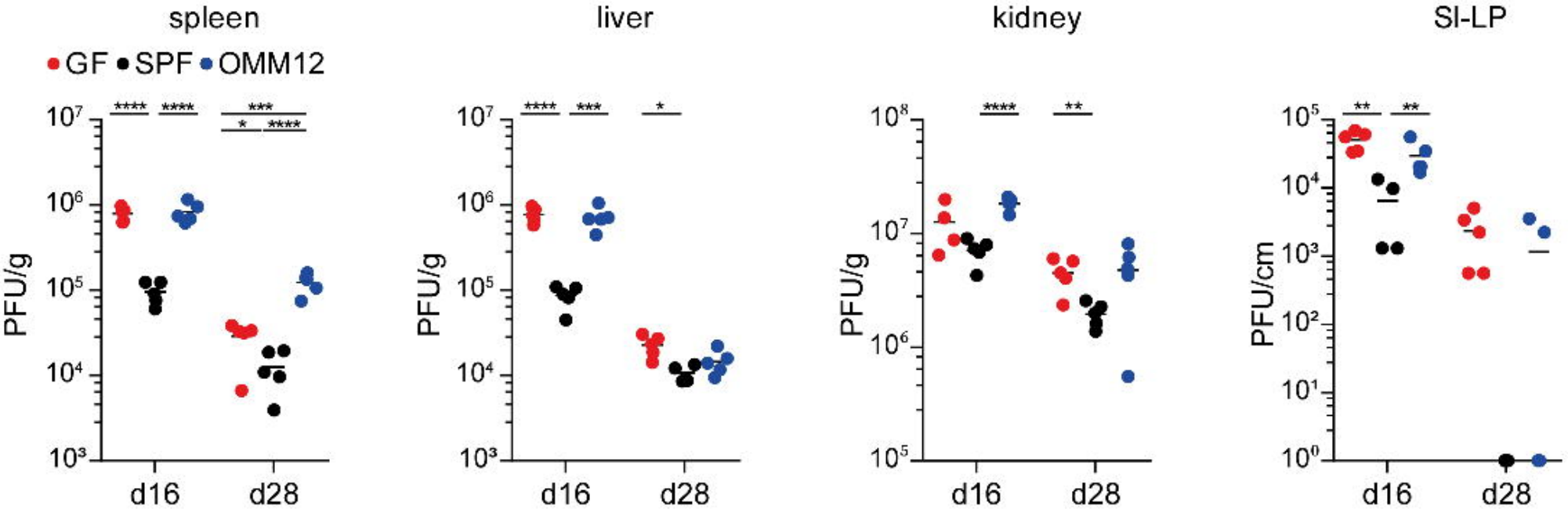
spleen
liver
kidney
SI-LP
GF
SPF
OMM12
PFU/g
PFU/cm
d16
d28
****
***
**
*